The Astronomical Journal, 140:1806–1813, 2010 December doi:10.1088/0004-6256/140/6/1806
© 2010. The American Astronomical Society. All rights reserved. Printed in the U.S.A.

COMET 169P/NEAT(=2002 EX_{12}): THE PARENT BODY OF THE α-CAPRICORNID METEOROID STREAM

Toshihiro Kasuga[1,3], David D. Balam[2], and Paul A. Wiegert[1]
[1] Department of Physics and Astronomy, The University of Western Ontario, 1151 Richmond Street London, ON N6A 3K7, Canada; tkasuga@uwo.ca
[2] Dominion Astrophysical Observatory, Herzberg Institute of Astrophysics, National Research Council Canada, Government of Canada, 5071 West Saanich Road, Victoria, BC, Canada
Received 2010 July 6; accepted 2010 September 7; published 2010 November 4

ABSTRACT

The Jupiter-family comet 169P/NEAT (previously known as asteroid 2002 EX_{12}) has a dynamical association with the α-Capricornid meteoroid stream. In this paper, we present photometric observations of comet 169P/NEAT to further investigate the physical characters of its disintegration state related to the stream. The comet shows a point-like surface brightness profile limiting contamination due to coma emission to ∼4% at most, indicating no evidence of outgassing. An upper limit on the fraction of the surface that could be sublimating water ice of $<10^{-4}$ is obtained with an upper limit to the mass loss of $\sim 10^{-2}$ kg s^{-1}. The effective radius of nucleus is found to be 2.3 ± 0.4 km. Red filter photometry yields a rotational period of 8.4096 ± 0.0012 hr, and the range of the amplitude 0.29 ± 0.02 mag is indicative of a moderately spherical shape having a projected axis ratio ∼1.3. The comet shows redder colors than the Sun, being compatible with other dead comet candidates. The calculated lost mass per revolution is $\sim 10^9$ kg. If it has sustained this mass loss over the estimated 5000 yr age of the α-Capricornid meteoroid stream, the total mass loss from 169P/NEAT ($\sim 10^{13}$ kg) is consistent with the reported stream mass ($\sim 10^{13}$–10^{15} kg), suggesting that the stream is the product of steady disintegration of the parent at every return.

Key words: comets: general – meteorites, meteors, meteoroids – minor planets, asteroids: general

Online-only material: color figures, machine-readable and VO tables

1. INTRODUCTION

Comet 169P/NEAT has been identified as the parent body of the α-Capricornid meteoroid stream (Brown et al. 2010; Jenniskens & Vaubaillon 2010). The semimajor axis, eccentricity, and inclination of 169P/NEAT are 2.604 AU, 0.767, and 11.°31, respectively (NASA JPL HORIZON), corresponding to a Tisserand parameter $T_J = 2.89$, and it is classified as a member of the Jupiter-family comets (JFCs; Levison 1996). The perihelion distance q ∼0.61 AU and the short orbital period $P_{\rm orb}$ ∼4.2 yr suggest the rapid sublimation of volatiles from the surface.

The typical timescale for losing ices from kilometer-sized nuclei of comets is shorter than the median dynamical lifetime of JFCs ($\tau_{\rm JFC} \sim 3.3 \times 10^5$ yr) (Levison & Duncan 1994), which implies a large number of dead or dormant JFCs should exist. Indeed, the number of dead or dormant comets "hidden" among the near-Earth object population has been estimated to be 6%–50% (Wetherill 1988; Harris & Bailey 1998; Fernández et al. 2001, 2002; Bottke et al. 2002; Weissman et al. 2002; DeMeo & Binzel 2008) and they are not easily distinguishable from ordinary asteroids (Jewitt 2004). An example is the nearly dead JFC: D/1819 W1(Blanpain) (recovered as asteroid 2003 WY_{25}), thought to be related to the Phoenicids meteoroid stream (Watanabe et al. 2005; Jenniskens & Lyytinen 2006; Sato & Watanabe 2010). It shows extremely weak coma activity in one of the smallest cometary nuclei ever (effective radius is 160 m) and has too small a mass-loss rate to supply the stream mass over the dynamical age of the stream (Jewitt 2006).

Asteroid 2002 EX_{12} was discovered by the NEAT survey in 2002. It was redesignated as 169P/NEAT in 2005 because it showed cometary appearance (Green 2005). On UT 2005 July 28 and 29, B. D. Warner observed a cometary tail using a 0.35 m Schmidt–Cassegrain reflector, and subsequently, A. Fitzsimmons also found such a tail (but no coma) on R-band images taken on July 29 at the 2.0 m Faulkes Telescope North at Haleakala, although no tail was in present in the data on May 10 and 14 (Warner & Fitzsimmons 2005). Warner (2006) measured its rotational period to be 8.369 ± 0.005 hr on the same nights in 2005, and recently, DeMeo & Binzel (2008) obtained the reflectance spectrum using the NASA Infrared Telescope Facility and found it is classified as a T-type based on the Bus taxonomy (Bus 1999) with an albedo $p_v = 0.03 \pm 0.01$.

Judged by the observations described above and the orbital association with the α-Capricornid meteoroid shower, 169P/NEAT is apparently a dying comet just before its extinction. In this paper, we present physical observations of 169P/NEAT, including limits on coma activity, mass-loss rate, fractional active area on the nucleus, size, rotational period, and colors.

2. OBSERVATIONS

Observations were carried out on the nights of UT 2010 February 17–19 and 22 using the Plaskett 1.85 m diameter parabolic mirror telescope at the Dominion Astrophysical Observatory (hereafter, DAO 1.8), which is located in Victoria, BC Canada (123.°24 24.′0 00.″0 W, 48.°0 37.′0 48.″0 N). An E2V 4608 × 2048 pixel charged-couple device camera was employed at the $f/5$ Newtonian focus. We used a 2 × 2 binned image scale 0.″62 pixel^{-1}, giving a field of view approximately 23.′9 × 10.′6.

Images were taken through both the Sloan Digital Sky Survey (SDSS) $u'g'r'i'z'$-filter system (Fukugita et al. 1996; Clen et al. 2007) and the Johnson R-filter (hereafter R_J) system with the telescope tracked non-sidereally to follow the motion of 169P/NEAT at rates of about 100″ hr^{-1}. A range of integration times from 30 s to 60 s was taken with each filter. Images were corrected by subtracting a bias image and dividing by a bias-subtracted flat-field image, the latter constructed from

[3] JSPS Postdoctoral Fellow for Research Abroad.

Table 1
Journal of Observations

UT Date	Integration (s)	Filter	r^a (AU)	Δ^b (AU)	α^c (deg)
2010 Feb 17	30	20 r'	1.4337	0.4728	16.10
2010 Feb 18	60	111 r'	1.4459	0.4862	16.20
2010 Feb 19	60	7 g', 7 r', 7 i', 3 z', 30 u'	1.4577	0.4993	16.35
2010 Feb 22	60	173 R_J	1.4936	0.5410	17.05

Notes.
[a] Heliocentric distance.
[b] Geocentric distance.
[c] Phase angle.

scaled, dithered images of the twilight sky in each filter. All images were calibrated using stars in the SDSS data release 7 (Abazajian et al. 2009) which were recorded in the same fields as 169P/NEAT (SDSS-J084308.95−012206.0, -J084238.89−004119.2, -J084225.72−000330.8, -J084157.70+000207.9, and -J084058.27+014453.9). While the SDSS standard stars were obtained with the R_J filter, we converted the SDSS catalog values into the case for R_J using the following relations (C. J. Pritchet of the CFHT Legacy Survey group 2002, private communication),

$$V = g' - 0.55(g' - r') - 0.03 \quad (1)$$

$$R_J = V - 0.59(g' - r') - 0.11. \quad (2)$$

The journal of observations is given in Table 1. The median FWHM varied from ∼2.″7 to 4.″0 through the observations. Object 169P/NEAT shows point-like images in our data (see Figure 1). Photometry was performed using synthetic circular apertures projected onto the sky. The photometric aperture radius used was twice the FWHM in the image (∼5.″4–8.″0) and the background sky brightness was determined within a concentric annulus having projected inner and outer radii of 14.″0 and 28.″0, respectively. Photometric results are listed in Tables 2 and 3.

3. OBSERVATIONAL RESULTS AND DISCUSSION

3.1. Surface Brightness

We modeled possible steady mass loss from 169P/NEAT using a seeing-convolution model (Luu & Jewitt 1992). For this purpose, we used 20 r'-band images taken on UT 2010 February 17 (Table 1), all free of background contamination. Individual images were rotated to be horizontal to the direction of the motion of 169P/NEAT and shifted using a fifth-order polynomial for pixel interpolation. The images of the background stars appear aligned and trailed in the data, which were then combined into a single image (total integration time of 600 s). The resulting refined image of 169P/NEAT has an FHWM of 2.″8 with a high signal-to-noise ratio: S/N $\geqslant$ 300 (see Figure 1). The seeing was determined from the point-spread function (PSF) of a field star and convolved with basic comet models of "nucleus plus coma." Model images are 100 × 100 pixels in size, representing the nucleus as a "point source" located at the central pixel and circularly symmetric comae of varying activity levels whose surface brightness varied inversely with distance from the nucleus. The parameter $\eta(\geqslant 0)$ defined by the ratio of the scattering cross sections of the coma and nucleus, which corresponds to the ratio of the flux densities scattered by the coma and by the nucleus cross section, was used to characterize coma-activity levels on preconvolution models. The case with $\eta = 0$ corresponds to no coma, while equal areas in the coma and the nucleus are expressed by $\eta = 1$ (Luu & Jewitt 1992).

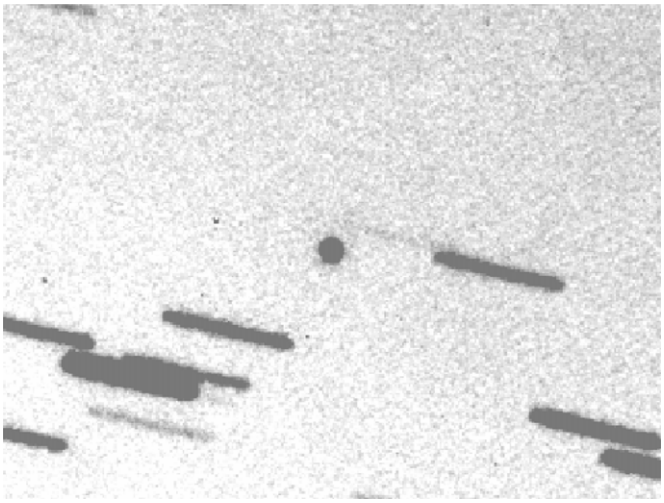

Figure 1. An r'-band image of 169P/NEAT taken at the Dominion Astrophysical Observatory 1.8 m telescope on UT 2010 February 17. The image is a composite of twenty 30 s integrations (total integration time of 600 s). The frame size is $200'' \times 150''$. No coma or tail is visible on the object having an FWHM of 2.″8.

Figure 2 compares normalized surface brightness profiles of 169P/NEAT, the star (solid line) and seeing-convolution models with coma levels of $\eta = 0.10$, 0.15, and 0.20 (dotted lines). We measured the PSF of 169P/NEAT in directions both parallel and perpendicular to the motion of the comet, the latter being used to determine the profile from trailed field star. Each profile was averaged along the rows over the entire width of the comet and the field star after subtracting sky background. Error bars show the result of uncertainty in the determination of the sky background adjustment to the object, suggesting that the activity level of 169P/NEAT is $\eta \lesssim 0.2$.

The normalized profiles of 169P/NEAT and the field star are very similar with tiny differences attributed to noise. To find the possible presence of coma, we used the relation given by Jewitt & Danielson (1984)

$$r_c'(\phi) = \Sigma(\phi) - 2.5\log(2\pi\phi^2), \quad (3)$$

where $r_c'(\phi)$ is the total magnitude of the coma inside a circle of radius ϕ in arcsec and $\Sigma(\phi)$ is the surface brightness at projected radius ϕ. The upper limit to the coma surface brightness at $\phi = 5.''6$ (double the seeing) can be set to be $\Sigma(5.''6) \geqslant 25.2$ mag arcsec^{-2}. Substitution into Equation (3) gives $r_c'(5.''6) > 19.4$ mag. This is 3.5 mag (factor of ∼25) fainter than the magnitude of the comet in the image used to measure the surface brightness profile, 15.9 mag in the r' band, meaning that a steady state coma can contribute at most a fraction $10^{0.4(r'-r_c'(5.6))} \sim 4\%$ of the total light from 169P/NEAT. Therefore, we conclude that the surface brightness profile of 169P/NEAT has little contamination from a steady state coma.

3.2. Size and Active Fractional Area

The results of the r'- and R_J-band photometry are summarized in Table 3. The r'-band filter was used on the nights of UT

Table 2
Color Photometry (UT 2010 February 19)

N	Midtime	$g'-r'$	$r'-i'$	$r'-z'$	u'	r'
1	30.36000					15.79 ± 0.02
2	30.39444	0.53 ± 0.02				15.79[a]
3	30.42861		0.17 ± 0.01			15.80[a]
4	30.46139			0.62 ± 0.03		15.80[a]
5	30.53222					15.80 ± 0.02
6	30.57000	0.51 ± 0.02				15.81[a]
7	30.60500		0.20 ± 0.01			15.81[a]
8	30.64056			0.79 ± 0.04		15.82[a]
9	30.67611					15.85 ± 0.02
10	30.70917	0.56 ± 0.02				15.83[a]
11	30.74389		0.22 ± 0.01			15.83[a]
12	30.81167					15.84 ± 0.01
13	30.84389	0.56 ± 0.02				15.85[a]
14	30.87778		0.26 ± 0.01			15.86[a]
15	30.94917					15.86 ± 0.02
16	31.00000	0.57 ± 0.02				15.88[a]
17	31.03417		0.24 ± 0.02			15.89[a]
18	31.10444					15.89 ± 0.02
19	31.13917	0.54 ± 0.02				15.91[a]
20	31.17472		0.24 ± 0.01			15.92[a]
21	31.21028			0.68 ± 0.04		15.93[a]
22	31.25472					15.95 ± 0.02
23	31.28778	0.56 ± 0.03				15.95[a]
24	31.32250		0.18 ± 0.02			15.96[a]
25	31.79653				18.03 ± 0.04[b]	...
Average colors		0.55 ± 0.02	0.22 ± 0.03	0.69 ± 0.09	18.03 ± 0.04	

Notes.
[a] r'-band magnitude interpolated from the light curve data set.
[b] The combined 30 u'-band image of 169P/NEAT with total integrations 1800 s.

Table 3
Red Filter Photometry

N	Date (UT 2010)	Midtime[a]	Filter	Apparent: R	Apparent: R_c[b]	Absolute: $R_c(1, 1, 0)$[c]
1	Feb 18	6.80139	r'	15.94 ± 0.02	15.72 ± 0.04	15.84 ± 0.04
2	Feb 18	6.82778	r'	15.96 ± 0.02	15.74 ± 0.04	15.86 ± 0.04
3	Feb 18	6.85417	r'	16.01 ± 0.02	15.79 ± 0.04	15.91 ± 0.04
4	Feb 18	6.88056	r'	15.99 ± 0.02	15.77 ± 0.03	15.89 ± 0.03
5	Feb 18	6.90694	r'	15.99 ± 0.02	15.77 ± 0.03	15.89 ± 0.03
6	Feb 18	6.93333	r'	15.99 ± 0.02	15.78 ± 0.03	15.89 ± 0.03
7	Feb 18	6.95972	r'	16.00 ± 0.02	15.78 ± 0.04	15.89 ± 0.04
8	Feb 18	6.98611	r'	15.93 ± 0.03	15.71 ± 0.04	15.83 ± 0.04
9	Feb 18	7.01250	r'	15.98 ± 0.02	15.76 ± 0.04	15.88 ± 0.04
10	Feb 18	7.03889	r'	16.01 ± 0.02	15.79 ± 0.04	15.91 ± 0.04

Notes.
[a] Time since UT 2010 February 18.00000. The middle of integration times is taken.
[b] Apparent magnitude converted into R_c-band data.
[c] Absolute red magnitude.

(This table is available in its entirety in machine-readable and Virtual Observatory (VO) forms in the online journal. A portion is shown here for guidance regarding its form and content.)

2010 February 18 and 19, and R_J-band filter was used on the night of UT 2010 February 22 because of a telescopic filter arrangement. All red images were converted into the Kron-Cousins filter system R_c (see again Table 3 and the Appendix).

The absolute red magnitude $R_c(1, 1, 0)$ is computed from the apparent red magnitude, R_c, using

$$R_c(1, 1, 0) = R_c - 5\log(r\,\Delta) - \beta\alpha, \quad (4)$$

where r and Δ are the heliocentric and geocentric distances (both in AU), α (deg) is the phase angle (Sun–Object–Earth), and β is the phase coefficient (mag deg^{-1}). We assumed the value $\beta = 0.04$ mag deg^{-1} that is typical for the nuclei of JFCs observed so far (Lamy et al. 2004).

The object's absolute magnitude $R_c(1,1,0)$ is related to the effective nucleus radius in meters, r_e, based on Russell (1916)

$$r_e[m] = \frac{1.496 \times 10^{11}}{\sqrt{p_R}} 10^{0.2(R_\odot - R_c(1,1,0))} \quad (5)$$

in which $R_\odot = -27.1$ is the apparent red magnitude of the Sun (Cox 2000). The albedo $p_v(\approx p_R) = 0.03 \pm 0.01$ was obtained

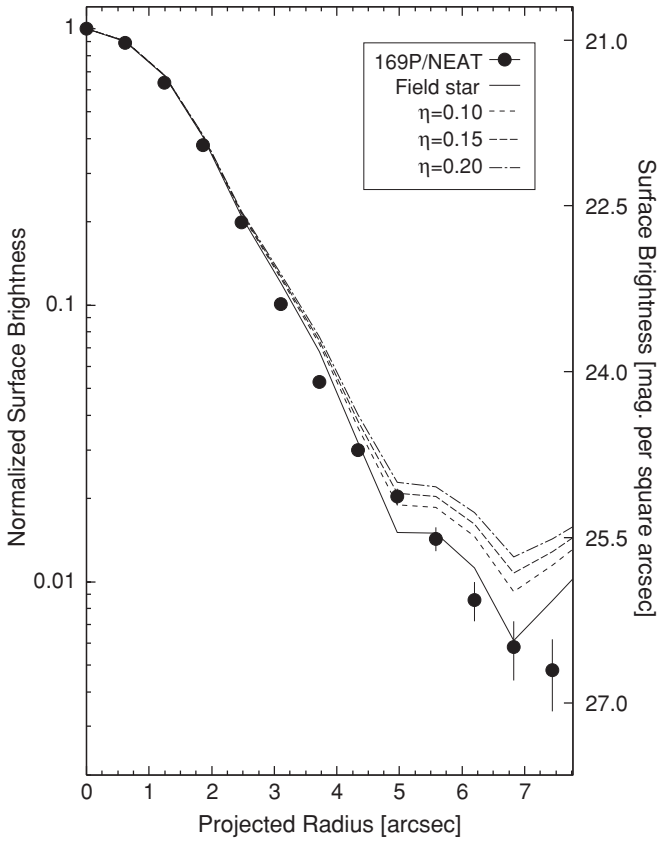

Figure 2. Normalized r'-band surface brightness profiles of 169P/NEAT, the field star, and seeing-convolution models having coma levels of $\eta = 0.10$, 0.15, and 0.20. One unit of the surface brightness of the comet is $\Sigma = 20.9$ mag arcsec^{-2}.

from the near-infrared observation of 169P/NEAT (DeMeo & Binzel 2008). Substitution into Equation (5), with the median $R_c(1, 1, 0) = 15.80 \pm 0.11$ (Table 3), then yields $r_e = 2.3 \pm 0.4$ km.

The comet 169P/NEAT shows point source-like surface brightness. From the observation we may estimate the maximum allowable coma activity. Under the assumption that volatile material (= water ice) still exists and occupied the nucleus surface, we can compute limits both to ongoing mass-loss rate and fractional active area on the surface. The approximate rate of the isotropic dust ejection from the object is formalized as a function of the parameter η (Section 3.1), and given by (Luu & Jewitt 1992)

$$\frac{dM}{dt} = \frac{1.0 \times 10^{-3} \pi \rho_{\rm grain} \bar{a} \eta r_e^2}{\theta r^{\frac{1}{2}} \Delta}, \quad (6)$$

where $\rho_{\rm grain} = 600$ kg m^{-3} is the assumed bulk density of the cometary grains (Weissman et al. 2004; A'Hearn et al. 2005), $\bar{a} = 0.5 \times 10^{-6}$ m is the assumed mean grain radius, $r_e = 2300 \pm 400$ m is the effective radius of 169P/NEAT, θ is the reference photometry aperture radius of 50 pixels (31″), and $r = 1.43$ AU, $\Delta = 0.47$ AU (Table 1). The calculated limit to the mass-loss rate is $dM/dt \lesssim 5.7 \pm 1.4 \times 10^{-2}$ kg s^{-1}, with $\eta \lesssim 0.2$. The active fraction on the nucleus surface, f, needed to supply dM/dt is calculated via (Luu & Jewitt 1992)

$$f = \frac{dM/dt}{4\pi r_e^2 \, dm/dt}, \quad (7)$$

where dm/dt is the specific sublimation mass-loss rate of water in kg m^{-2} s^{-1}. The dust-to-gas ratio is assumed to be 1 (Greenberg 1998; Luu & Jewitt 1992) and dm/dt is calculated from the energy-balance equation

$$\frac{S_\odot (1 - A)}{r^2} = \chi [\epsilon \sigma T^4 + L(T) dm/dt] \quad (8)$$

in which $S_\odot = 1365$ W m^{-2} is the solar constant, r (in AU) is the heliocentric distance, $\epsilon = 0.9$ is the wavelength-averaged emissivity, $\sigma = 5.67 \times 10^{-8}$ W m^{-2} K^{-4} is the Stephan–Boltzmann constant, and T [K] is the equilibrium temperature. $A = 0.009$ ($= p_v q$) is the Bond albedo, where $p_v \approx 0.03$ (DeMeo & Binzel 2008) and $q \approx 0.3$ is the phase integral suggested by the studies of cometary nuclei and Jupiter Trojan asteroids (Fernández et al. 2003; Buratti et al. 2004). The latent heat of sublimation for water at temperature T [K] can be expressed by $L(T) = (2.875 \times 10^6)$–$(1.111 \times 10^3)T$ in J kg^{-1}, taking the polynomial fit to the thermodynamic data in Delsemme & Miller (1971). The parameter χ represents the distribution of incident solar power across the surface of the nucleus in which $\chi = 1$ corresponds to a flat plate oriented perpendicular to the Sun, $\chi = 2$ to an isothermal hemisphere and $\chi = 4$ to an isothermal sphere.

The specific sublimation mass-loss rate can be derived iteratively using the temperature-dependent water vapor pressure given by Fanale & Salvail (1984). A maximum value of $\chi = 4$ (an isothermal sphere) provides a maximum active fractional area with the minimum specific sublimation mass-loss rate. At 1.43 AU, Equations (7) and (8) give $f = 2.3 \pm 0.8 \times 10^{-5}$ ($f < 10^{-4}$ with more than 5σ level of significance), and $dm/dt = 3.8 \times 10^{-5}$ kg m^{-2} s^{-1} at a temperature of 189 K.

In general, typical low active surface fractional areas of $10^{-3} \leqslant f \leqslant 10^{-2}$ are indicated by observations of about 100 comets (A'Hearn et al. 1995; Tancredi et al. 2006). If comets have $f \ll 10^{-3}$, they are difficult to distinguish from asteroids owing to the difficulty of detecting very faint coma activity (Luu & Jewitt 1992). The small active surface fraction of 169P/NEAT with upper limits of $f < 10^{-4}$ is much less than any other comet and no significant coma is presently found, suggesting the existence of refractory surface mantle (A'Hearn et al. 1995).

3.3. Rotational Period and Shape

The photometric data (Table 3) show systematic variations that are larger than the measurement errors. The variation is likely due to rotation. To find the rotational period for 169P/NEAT, we used the spectral analysis technique that employs the Discrete Fourier Transform algorithm (Lomb 1976; Scargle 1982). In this method, the spectral power as a function of angular frequency is evaluated by the quality of the fit at a given frequency in the data. The frequency with the maximum power shows the highest significance level, which is taken to reflect the most likely periodicity in the data. The expected light curves of minor bodies in the solar system are double-peaked, produced by an asymmetric and elongated shape, which we also assumed for 169P/NEAT. The results of the spectral analysis are summarized in Figure 3. The amplified view around the peak is shown as well. The frequency spacing is about $\Delta\nu \approx 1/50{,}000$ rotations day^{-1}. The highest peak occurs near the frequency $\nu = 2.85388$ rotations day^{-1} ($P_{\rm rot} = 0.3504$ day), therefore we conclude that the true double-peaked rotational period of 169P/NEAT is $P_{\rm rot} = 8.4096$ hr (Figure 4). The uncertainty

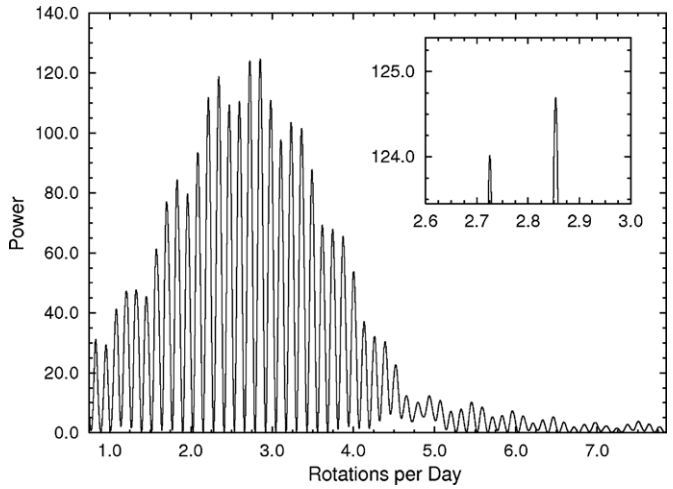

Figure 3. Spectral analysis curve for the 169P/NEAT $R_c(1,1,0)$ data. The peak near 2.854 rotation day^{-1} ($P_{\rm rot} = 0.3504$ day^{-1}) is taken to be the best estimate of the light curve period.

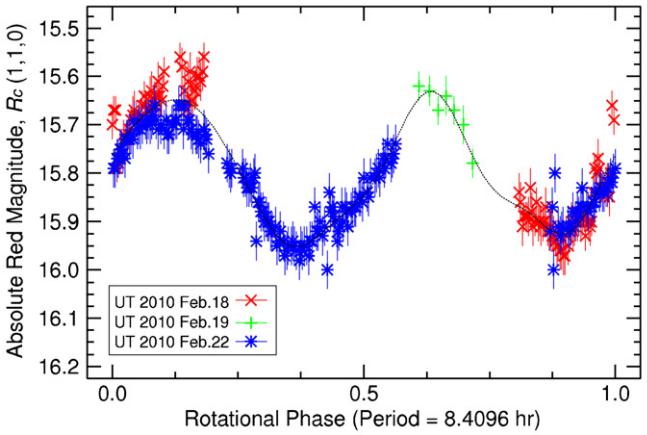

Figure 4. Red photometry of 169P/NEAT observed on UT 2010 February 18, 19, and 22, phased to the double-peak period $P_{\rm rot} = 8.4096 \pm 0.0012$ hr. Dotted curve displays fitting result having the amplitude $\Delta R_c(1,1,0) = 0.29 \pm 0.02$.
(A color version of this figure is available in the online journal.)

on the period is estimated by the acceptable range of frequency given by the significant level, $2.85349 \leqslant \nu \leqslant 2.85427$ (8.4085 hr $\leqslant P_{\rm rot} \leqslant$ 8.4108 hr), producing an estimated error of $\pm$0.0012 hr.

The light curve fitting reveals the maximum photometric range of 169P/NEAT to be $\Delta R_c(1, 1, 0) = 0.29 \pm 0.02$. This gives a lower limit to the intrinsic axis ratio, a/b, between long axis a and short axis b. Assuming the object's rotation axis is perpendicular to our line of sight, the ratio is expressed as $10^{0.4\Delta R_c(1,1,0)}$. We find $a/b = 1.31 \pm 0.03$. Our observations of 169P/NEAT indicate a more sphere-like shape than typical of cometary nuclei which often are elongated bodies with $a/b \geqslant 1.5$ (Jewitt 2004). Albedo differences on the surface of JFC nuclei (examples: 19P/Borrelly and 9P/Tempel 1) also could cause a significant part of this light curve amplitude (Buratti et al. 2004; Lamy et al. 2007; Li et al. 2007a, 2007b). Under the assumption that 169P/NEAT is held together against rotational disruption only by its own gravity, a minimum density $\rho_{\rm min}$ for 169P/NEAT can be derived from $\rho_{\rm min} = 1000\ (3.3\ {\rm hr}/{\rm P_{rot}})^2 (a/b)$ using $P_{\rm rot}$ in hours and its axis ratio (Harris 1996; Pravec & Harris 2000), giving $\rho_{\rm min} = 200$ kg m^{-3}. A density lower limit for typical JFC nuclei is estimated to be near 600 kg m^{-3} with a couple of dozens samples (Lowry & Weissman 2003; Jewitt & Sheppard 2004; Snodgrass et al. 2006, 2008), and the work of Jewitt & Sheppard (2004) implies that their rotationally stable conditions would require a density of over 500 kg m^{-3}. According to those statistical results, the density of 169P/NEAT is apparently lower (half or less) than typical JFC nuclei and its rotation is likely to be unstable.

It should be noted that observations of 169P/NEAT taken by Warner (2006) on the nights of UT 2005 July 28 and 29 gave $P_{\rm rot} = 8.369 \pm 0.005$ hr and $a/b \sim 1.45$ (asymmetric double-peaked light curve shape), which do not match our measurements even considering errors. Possibly, non-principal axis rotation of 169P/NEAT may be inferred from those of differences. Much more likely for cometary nuclei, non-central outgassing could generate torques that change the angular momentum of nucleus (spin period) and the object could be driven into an excited rotational state (Jewitt 1997). Simultaneously, and acting in opposition to this, the related motion creates periodic internal friction in the nucleus, leading the nucleus back to the minimum rotational energy state (damping of spin). Here, we calculated the timescale for rotational excitation $\tau_{\rm ex}$ (Jewitt 1997) to find if the state is ongoing, and the critical object radius needed to remain in the excited state taking timescales of excitation and damping (Burns & Safronov 1973) to be equal, then

$$\tau_{\rm ex} \approx \frac{\omega \rho_{\rm n} r_e^4}{V_{\rm th} k_T\, dM/dt} \tag{9}$$

$$r_{\rm cr}[m] \leqslant \left(4\pi\, \frac{\mu Q V_{\rm th} k_T f}{\rho_{\rm n}^2 K_3^2 \omega^4} dm/dt \right)^{1/4}, \tag{10}$$

where $\omega = 2\pi/P_{\rm rot}$ is the angular spin rate corresponding to rotational period, $\rho_{\rm n}$ ($= \rho_{\rm grain} = 600$ kg m^{-3}) is the density of the nucleus, $V_{\rm th}$ is the assumed mass-weighted outflow speed (Samarasinha et al. 1986; Jewitt 1991), k_T is the dimensionless moment arm for the torque (Jewitt 1997), μ (N m^{-2}) is the rigidity, Q is the quality factor (fractional loss of energy per cycle), and K_3 is the shape-dependent numerical factor. We followed Harris (1994) and took $\mu Q = 5.0 \times 10^{11}$ (N m^{-2}) and ${K_3}^2 \approx 0.03$ (based on the data for Phobos). $V_{\rm th} = 500/\sqrt{r}$ ($r = 1.43$ AU given by Table 1) was used (Jewitt 1991, 2002), and the dimensionless moment arm has been estimated $0.01 \leqslant k_T \leqslant 0.05$ (Jewitt 1997; Gutiérrez et al. 2003), so we adopted those of the median value $k_T = 0.025$. Other parameters are given earlier ($dM/dt \sim 5.7 \times 10^{-2}$ kg s^{-1}, $f \sim 2.3 \times 10^{-5}$). We have found $\tau_{\rm ex} \sim 1.9 \times 10^5$ yr $< \tau_{\rm JFC}$ and $r_{\rm e}$(2.3 km) $< r_{\rm cr}$ (7.3 km), suggesting 169P/NEAT could maintain non-principal axis rotation.

Next, we focused on the difference in the rotational period $\Delta P_{\rm rot} \sim 0.041$ hr since 2005. This corresponds to ~4.5 yr, which is almost consistent with $P_{\rm orb}$ of 169P/NEAT. The mass loss resulting in the fractional change in the spin angular velocity $\Delta P_{\rm rot}/P_{\rm rot}$ can be computed using the equation given by Jewitt (1997)

$$\frac{\Delta P_{\rm rot}}{P_{\rm rot}} = k_T \left(\frac{\Delta M}{M} \right) \left(\frac{V_{\rm th}}{V_{\rm eq}} \right). \tag{11}$$

In which $V_{\rm eq} (= r_{\rm e}\omega)$ is the equatorial velocity and $\Delta M/M$ is the fractional change in the mass, yielding a mass loss from 169P/NEAT of $\Delta M \sim 7.0 \times 10^9$ kg per orbit. This can be compared with the total mass in the α-Capricornids meteoroid stream. The stream has a dynamical age of ~5000 yr

Table 4
Color Results of 169P/NEAT

$B-V$	$V-R_c$	R_c-I_c	$B-I_c$	$U-B$	References[a]
0.71 ± 0.04	0.41 ± 0.03	0.39 ± 0.06	1.52 ± 0.08	···	2, 3
0.69 ± 0.04	0.41 ± 0.03	0.43 ± 0.06	1.53 ± 0.08	···	6, 7
0.74 ± 0.04	0.44 ± 0.04	0.44 ± 0.07	1.62 ± 0.09	···	10, 11
0.74 ± 0.05	0.45 ± 0.04	0.49 ± 0.07	1.68 ± 0.10	···	13, 14
0.75 ± 0.05	0.45 ± 0.04	0.46 ± 0.07	1.66 ± 0.09	···	16, 17
0.72 ± 0.04	0.44 ± 0.04	0.47 ± 0.07	1.63 ± 0.09	···	19, 20
0.74 ± 0.05	0.43 ± 0.03	0.41 ± 0.06	1.57 ± 0.09	···	23, 24
···	···	···	···	0.17 ± 0.06[b]	25

Notes.
[a] N in Table 2.
[b] B-band data are extrapolated to the midtime 31.79653.

and the total mass is $\sim 10^{13}$–10^{15} kg (Jenniskens & Vaubaillon 2010). Assuming the observed mass loss from 169P/NEAT is comparable at each return, in several thousand years the accumulated stream mass ought to be $\sim 10^{13}$ kg (8.3×10^{12} kg). Therefore, the origin of the α-Capricornids meteoroid stream could be formed by steady disintegration of the parent, not by a catastrophic breakup as in the case for the Geminid parent (Ohtsuka et al. 2006, 2008; Jewitt & Hsieh 2006; Kasuga & Jewitt 2008).

3.4. Colors

Table 4 shows the color results for 169P/NEAT in the BVR_cI_c-filter system, which were transformed from the data taken by the SDSS filter system on the night of UT 2010 February 19 (see the Appendix).

Figure 5 presents the color distributions of $V-R_c$ versus $B-I_c$ for the various families of pristine bodies in the solar system (Lamy & Toth 2009; Hsieh et al. 2004, 2009, 2010; Jewitt et al. 2009). Additionally, we used the $V-R_c$ color index to derive the normalized spectral gradient, S', via

$$(V-R_c) = (V-R_c)_\odot + 2.5\log\left[\frac{2+S'\Delta\lambda}{2-S'\Delta\lambda}\right], \quad (12)$$

(Luu & Jewitt 1990), where $(V-R_c)_\odot$ is the color index of the Sun (= 0.36) in the Kron-Cousins system, S' is in %(1000 Å)$^{-1}$, and $\Delta\lambda$ is the difference between the V- and R_c-band center wavelengths, i.e., 1000 Å (from 5500 Å to 6500 Å). Table 5 summarizes the data.

The colors of 169P/NEAT are more compatible with those of dead comets within the uncertainties, rather than Jupiter Trojans that are spectrally similar to the D-type asteroids (Jewitt & Luu 1990; Fornasier et al. 2007; Karlsson et al. 2009). The main belt comets (MBCs) are predominantly C-type asteroids, which show more neutral colors than 169P/NEAT (Hsieh et al. 2004, 2009, 2010; Jewitt et al. 2009). We note that 169P/NEAT's color indices are much less red than those of ecliptic cometary (EC) nuclei, suggesting a different evolution stage of the surface of the object. The low activity in the present data provides confidence that the measured colors refer to the nucleus alone. The colors are flatter than the ECs' nucleus, probably because the nucleus of 169P/NEAT's surface has a refractory mantle that has evolved more than ECs and Kuiper Belt Objects (KBOs) because of the missing red matter (Jewitt 2002). This means, a rubble mantle is to be expected on 169P/NEAT rather than the ballistic type formed by resurfacing after past outgassing of volatiles. Jewitt (2002, 2004) provides the models to infer the timescales for the

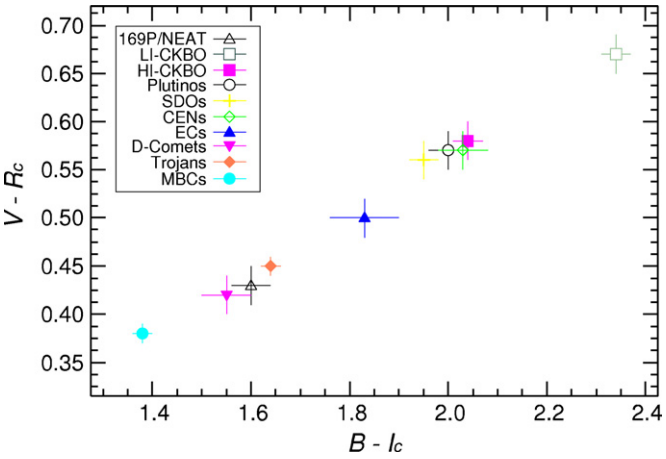

Figure 5. Color distributions $B-I_c$ vs. $V-R_c$ for 169P/NEAT and various types of minor bodies in the solar system; LI-CKBO, HI-CKBO, Plutinos, SDOs, CENs, D-Comets, Trojan (Lamy & Toth 2009, and references therein), and MBCs (Hsieh et al. 2004, 2009, 2010; Jewitt et al. 2009) (see Section 3.4 and Table 5).
(A color version of this figure is available in the online journal.)

rubble mantle growth τ_M and the loss of volatiles from mantled cometary nuclei τ_{dv},

$$\tau_M \sim \frac{\rho_n L_D}{f_M dm/dt} \quad (13)$$

$$\tau_{dv} \sim \frac{\rho_n r_e}{f_M (dm/dt)_{\rm mean}}, \quad (14)$$

in which $(dm/dt)_{\rm mean} \sim 10^{-5}$ kg m^{-2} s^{-1} is the assumed specific mass loss averaged around typical JFC orbit (Jewitt 2004). L_D ($\sim \sqrt{\kappa P_{\rm rot}}$) is the diurnal thermal skin depth determined by the thermal diffusivity of porous dielectric materials ($\kappa \sim 10^{-7}$ m^2 s^{-1}) and rotational period of the object, corresponding to ~6 cm for 169P/NEAT. The parameter f_M is the rubble mantle fraction (fraction of the solid matter in the nucleus too large to be ejected by gas drag) calculated from the power-law-type dust size distribution and the critical radius of grain size (a_c) that is to remain on the nucleus surface. Assuming the size distribution is consistent with P/Halley (power law to the fourth power), f_M for 169P/NEAT is found to be ~0.04 and $a_c \sim 5$ cm. As a result $\tau_M \sim 0.7$ yr and $\tau_{dv} \sim 1.0 \times 10^5$ yr. The former is much shorter than $P_{\rm orb}$ and the latter is also quicker than $\tau_{\rm JFC}$. Therefore, we conclude that 169P/NEAT is inactive during most of its orbit owing to rubble mantle formation and would be highly

Table 5
Distribution of Optical Colors of 169P/NEAT and Different Types of Small Bodies

169P/NEAT and Families	$B-V$	$V-R_c$	R_c-I_c	$B-I_c$	S'	Source
169P/NEAT	0.73 ± 0.02	0.43 ± 0.02	0.44 ± 0.04	1.60 ± 0.06	6.7 ± 1.6[a]	(1)
LI-CKBO[b]	1.04 ± 0.02	0.67 ± 0.02	0.63 ± 0.02	2.34 ± 0.03	28.4 ± 1.8	(2)
HI-CKBO[c]	0.92 ± 0.02	0.58 ± 0.02	0.54 ± 0.02	2.04 ± 0.03	20.2 ± 1.8	(2)
Plutinos[d]	0.89 ± 0.03	0.57 ± 0.02	0.54 ± 0.02	2.00 ± 0.04	19.3 ± 1.8	(2)
SDOs[e]	0.87 ± 0.02	0.56 ± 0.02	0.52 ± 0.02	1.95 ± 0.03	18.4 ± 1.8	(2)
CENs[f]	0.89 ± 0.04	0.57 ± 0.02	0.57 ± 0.03	2.03 ± 0.05	19.3 ± 1.8	(2)
ECs[g]	0.88 ± 0.06	0.50 ± 0.02	0.45 ± 0.02	1.83 ± 0.07	12.9 ± 1.8	(2)
D-Comets[h]	0.73 ± 0.02	0.42 ± 0.02	0.40 ± 0.04	1.55 ± 0.05	5.5 ± 1.8	(2)
Trojans[i]	0.77 ± 0.01	0.45 ± 0.01	0.42 ± 0.01	1.64 ± 0.02	8.3 ± 0.9	(2)
MBCs[j]	0.64 ± 0.02	0.38 ± 0.01	0.36 ± 0.05	1.38 ± 0.02	1.4 ± 0.9	(3)
Solar colors	0.63	0.36	0.33	1.32	...	(4)

Notes.
[a] Given by Table 4.
[b] Classical Kuiper Belt Objects (KBOs) with low inclination $i < 4°$.
[c] Classical Kuiper Belt Objects (KBOs) with high inclination $i > 4°$.
[d] Resonant KBOs.
[e] Scattered KBOs.
[f] Centaurs.
[g] Ecliptic cometary nuclei ($2 < T_J < 3$ and $T_J > 3$ with $a < a_J$(5.2 AU)).
[h] Dead comets candidates: Interpolated data originated from Jewitt (2002): $V - R_c = 0.44 \pm 0.02$, $S' = 7.0 \pm 2.0$.
[i] Jupiter Trojans.
[j] Main belt comets.
References. (1) This work; (2) Lamy & Toth 2009, and references therein; (3) Hsieh et al. 2004; Jewitt et al. 2009; Hsieh et al. 2009, 2010; (4) Hardorp 1982; Hartmann 1987; Tueg & Schmidt-Kaler 1982.

devolatilized. An open question that still remains is whether the volatiles are depleted down to the core, or just a few times the thermal skin depth below the surface until excavating the mantle (Jewitt et al. 2009). In future, a NASA Deep Impact like collisional mission applied to 169P/NEAT would be valuable to better understand the puzzling evolutional stages in both the surface and the interior of dead comets broadly, and such an impact may produce artificial α-Capricornids meteoroid streams (A'Hearn et al. 2005; Kasuga et al. 2006).

4. SUMMARY

Optical observations of comet 169P/NEAT lead to the following results.

1. The surface brightness shows a star-like profile, setting a limit to the fractional light scattered by the steady state coma of 0%–4%.
2. The absolute red magnitude of the nucleus is $R_c(1,1,0) = 15.80 \pm 0.11$ (using an assumed value of linear phase coefficient $\beta = 0.04$). The geometric albedo of the 169P/NEAT ($p_R = 0.03 \pm 0.01$) provides the effective radius $r_e = 2.3 \pm 0.4$ km.
3. No evidence of lasting mass loss was found from the surface brightness profiles in imaging data. The maximum mass-loss rate is $\sim 10^{-2}$ kg s^{-1} which corresponds to the fractional active area $f < 10^{-4}$.
4. 169P/NEAT might be in non-principal axis rotation with the period of $P_{\rm rot} = 8.4096 \pm 0.0012$ hr if the light curve has two maxima per period. The photometric range of $\Delta R_c = 0.29 \pm 0.02$ mag corresponds to an axis ratio of 1.31 ± 0.03 with the critical density $\geqslant 200$ kg m^{-3}.
5. The α-Capricornid meteoroid stream was probably formed by the steady mass loss from the parent because the calculated lost mass per revolution $\Delta M \sim 10^9$ kg is in agreement with the total mass of the stream for about a 5000 yr dynamical lifetime.
6. Optical colors measured for 169P/NEAT are less red than usual cometary nuclei and Trojans, but similar to those of dead comet candidates.

T.K. thanks David Jewitt for creative discussions and input to this study. T.K. also thanks Margaret Campbell-Brown and Reto Musci at the University of Western Ontario for helpful comments on this research. We appreciate Budi Dermawan for his assistance with the light curve analysis. Support for this work is provided by the JSPS Research Abroad Fellowships for young scientists to T.K., and also by the Natural Sciences and Engineering Research Council of Canada. Finally, we are grateful to the anonymous reviewer who offered valuable suggestions to improve this work.

APPENDIX

FILTER SYSTEMS TRANSFORMATIONS

We carried out observations using both the SDSS filter system ($u'g'r'i'z'$-filters) and the Johnson R (R_J-filter) for the present studies. For consistency with the published literature, we converted our results to the Johnson–Kron-Cousins filter system ($UBVR_cI_c$-filters) in this study. Here, we show transformations between those systems.

The SDSS systems were transformed using equations given by Chonis & Gaskell (2008):

$$B = g' + (0.327 \pm 0.047)(g' - r') + (0.216 \pm 0.027) \quad \text{(A1)}$$

$$V = g' - (0.587 \pm 0.022)(g' - r') - (0.011 \pm 0.013) \quad \text{(A2)}$$

$$R_c = r' - (0.272 \pm 0.092)(r' - i') - (0.159 \pm 0.022) \quad \text{(A3)}$$

$$I_c = i' - (0.337 \pm 0.191)(r' - i') - (0.370 \pm 0.041) \quad \text{(A4)}$$

$$U = u' - 0.854 \pm 0.007. \quad \text{(A5)}$$

We used the relationship between Johnson and Kron-Cousins (Fernie 1983)

$$(V - R_c) = 0.730 \pm 0.009(V - R_J) - 0.024 \pm 0.004. \quad \text{(A6)}$$

The data set in Table 2 was substituted into Equations (A1)–(A5), in order to obtain 169P/NEAT's colors (see Table 4). For converting into the Kron-Cousins system R_c, we adopted $(r' - i') = 0.22 \pm 0.03$ in Equation (A3) for the SDSS system, while R_J (Table 3) and the averaged value $V = 16.08 \pm 0.03$ (given by the A2) were used in Equation (A6). The resulting red color photometry in the R_c is summarized in Table 3.

REFERENCES

Abazajian, K. N., et al. 2009, ApJS, 182, 543
A'Hearn, M. F., Millis, R. L., Schleicher, D. G., Osip, D. J., & Birch, P. V. 1995, Icarus, 118, 223
A'Hearn, M. F., et al. 2005, Science, 310, 258
Bottke, W. F., Jr., Morbidelli, A., Jedicke, R., Petit, J.-M., Levison, H., Michel, P., & Metcalfe, T. S. 2002, Icarus, 156, 399
Brown, P., Wong, P. D., Weryk, R. J., & Wiegert, P. 2010, Icarus, 207, 66
Buratti, B. J., Hicks, M. D., Soderblom, L. A., Britt, D., Oberst, J., & Hillier, J. K. 2004, Icarus, 167, 16
Burns, J. A., & Safronov, V. S. 1973, MNRAS, 165, 403
Bus, S. J. 1999, PhD Thesis, Massachusetts Institute of Technology
Chonis, T. S., & Gaskell, C. M. 2008, AJ, 135, 264
Clem, J. L., Vanden, B. D. A., & Stetson, P. B. 2007, AJ, 134, 1890
Cox, A. N. 2000, Allen's Astrophysical Quantities (New York: Springer)
Delsemme, A. H., & Miller, D. C. 1971, Planet. Space Sci., 19, 1229
DeMeo, F., & Binzel, R. P. 2008, Icarus, 194, 436
Fanale, F. P., & Salvail, J. R. 1984, Icarus, 60, 476
Fernández, J. A., Gallardo, T., & Brunini, A. 2002, Icarus, 159, 358
Fernández, Y. R., Jewitt, D. C., & Sheppard, S. S. 2001, ApJ, 553, L197
Fernández, Y. R., Sheppard, S. S., & Jewitt, D. C. 2003, AJ, 126, 1563
Fernie, J. D. 1983, PASP, 95, 782
Fukugita, M., Ichikawa, T., Gunn, J. E., Doi, M., Shimasaku, K., & Schneider, D. P. 1996, AJ, 111, 1748
Fornasier, S., Dotto, E., Hainaut, O., Marzari, F., Boehnhardt, H., de Luise, F., & Barucci, M. A. 2007, Icarus, 190, 622
Green, D. W. E. 2005, IAU Circ., 8591, 3
Greenberg, J. M. 1998, A&A, 330, 375
Gutiérrez, P. J., Jorda, L., Ortiz, J. L., & Rodrigo, R. 2003, A&A, 406, 1123
Hardorp, J. 1982, A&A, 105, 120
Harris, A. W. 1994, Icarus, 107, 209
Harris, A. W. 1996, Lunar and Planetary Sci., 27, 493
Harris, N. W., & Bailey, M. E. 1998, MNRAS, 297, 1227
Hartmann, W. K., Tholen, D. J., & Cruikshank, D. P. 1987, Icarus, 69, 33
Hsieh, H. H., Jewitt, D. C., & Fernández, Y. R. 2004, AJ, 127, 2997
Hsieh, H. H., Jewitt, D. C., & Ishiguro, M. 2009, AJ, 137, 157
Hsieh, H. H., Jewitt, D., Lacerda, P., Lowry, S. C., & Snodgrass, C. 2010, MNRAS, 403, 363
Jenniskens, P., & Lyytinen, E. 2006, AJ, 130, 1286
Jenniskens, P., & Vaubaillon, J. 2010, AJ, 139, 1822
Jewitt, D. 1991, in Comets in the Post-Halley Era, ed. R. L. Newburn, Jr. M. Neugebauer, & J. Rahe (Dordrecht: Kluwer), 19
Jewitt, D. 1997, Earth Moon Planets, 79, 35
Jewitt, D. 2006, AJ, 131, 2327
Jewitt, D. 2009, in Small Bodies in Planetary Systems, ed. I. Mann, A. Nakamura, & T. Mukai (Lecture Notes in Physics, Vol. 758; Heidelberg: Springer), 259
Jewitt, D., & Danielson, G. E. 1984, Icarus, 60, 435
Jewitt, D., & Hsieh, H. H. 2006, AJ, 132, 1624
Jewitt, D., & Sheppard, S. 2004, AJ, 127, 1784
Jewitt, D., Yang, B, & Haghighipour, N. 2009, AJ, 137, 4313
Jewitt, D. C. 2002, AJ, 123, 1039
Jewitt, D. C. 2004, in Comets II, Vol. 745, ed. M. C. Festou, H. U. Keller, & H. A. Weaver (Tucson, AZ: Univ. Arizona Press), 659
Jewitt, D. C., & Luu, J. X. 1990, AJ, 100, 933
Karlsson, O., Lagerkvist, C.-I., & Davidsson, B. 2009, Icarus, 199, 106
Kasuga, T., & Jewitt, D. 2008, AJ, 136, 881
Kasuga, T., Watanabe, J., & Sato, M. 2006, MNRAS, 373, 1107
Lamy, P., & Toth, I. 2009, Icarus, 201, 674
Lamy, P. L., Toth, I., A'Hearn, M. F., Weaver, H. A., & Jorda, L. 2007, Icarus, 187, 132
Lamy, P. L., Toth, I., Fernandez, Y. R., & Weaver, H. A. 2004, in Comets II, Vol. 745, ed. M. C. Festou, H. U. Keller, & H. A. Weaver (Tucson, AZ: Univ. Arizona Press), 223
Levison, H. F. 1996, in ASP Conf. Ser. 107, Completing the Inventory of the Solar System, ed. T. W. Rettig & J. M. Hahn (San Francisco, CA: ASP), 173
Levison, H. F., & Duncan, M. J. 1994, Icarus, 108, 18
Li, J.-Y., A'Hearn, M. F., McFadden, L. A., & Belton, M. J. S. 2007a, Icarus, 188, 195
Li, J.-Y., et al. 2007b, Icarus, 187, 41
Lomb, N. R. 1976, Ap&SS, 39, 447
Lowry, S. C., & Weissman, P. R. 2003, Icarus, 164, 492
Luu, J. X., & Jewitt, D. C. 1990, AJ, 100, 913
Luu, J. X., & Jewitt, D. C. 1992, Icarus, 97, 276
Ohtsuka, K., Ito, T., Arakida, H., & Yoshikawa, M. 2008, M&PSA, 43, 5055
Ohtsuka, K., Sekiguchi, T., Kinoshita, D., Watanabe, J. I., Ito, T., Arakida, H., & Kasuga, T. 2006, A&A, 450, L25
Pravec, P., & Harris, A. W. 2000, Icarus, 148, 12
Russell, H. N. 1916, ApJ, 43, 173
Samarasinha, N. H., A'Hearn, M. F., Hoban, S., & Klinglesmith, D. A., III 1986, in ESA Proc. 20th ESLAB Symposium on the Exploration of Halley's Comet, Vol. 1, ed. B. Battrick, E. J. Rolfe, & R. Reinhard (ESA SP-250; Paris: ESA), 487
Sato, M., & Watanabe, J. 2010, PASJ, 62, 509
Scargle, J. D. 1982, ApJ, 263, 835
Snodgrass, C., Lowry, S. C., & Fitzsimmons, A. 2006, MNRAS, 373, 1590
Snodgrass, C., Lowry, S. C., & Fitzsimmons, A. 2008, MNRAS, 385, 737
Tancredi, G., Fernández, J. A., Rickman, H., & Licandro, J. 2006, Icarus, 182, 527
Tueg, H., & Schmidt-Kaler, T. 1982, A&A, 105, 400
Warner, B. D. 2006, Bull. Minor Planets Sect. Ass. Lunar Plan. Obs., 33, 35
Warner, B. D., & Fitzsimmons, A. 2005, IAU Circ., 8578, 1
Watanabe, J., Sato, M., & Kasuga, T. 2005, PASJ, 57, L45
Weissman, P. R., Asphaug, E., & Lowry, S. C. 2004, in Comets II, Vol. 745, ed. M. C. Festou, H. U. Keller, & H. A. Weaver (Tucson, AZ: Univ. Arizona Press), 337
Weissman, P. R., Bottke, W. F., Jr., & Levison, H. F. 2002, in Asteroids III, ed. W. F. Bottke Jr., A. Cellino, P. Paolicchi, & R. P. Binzel (Tucson, AZ: Univ. Arizona Press), 669
Wetherill, G. W. 1988, Icarus, 76, 1